Construction and Building Materials 404 (2023) 133142

Contents lists available at ScienceDirect

Construction and Building Materials

journal homepage: www.elsevier.com/locate/conbuildmat

Effects of bacteria-based self-healing nutrients on hydration and rheology of cement pastes

Adonay Pinto, Belén González-Fonteboa *, Sindy Seara-Paz, Fernando Martínez-Abella

Department of Civil Engineering, University of A Coruna. Campus de Elvina, 15008 A Coruna, Spain

ARTICLE INFO

Keywords:
Yeast extract
Calcium lactate
Calcium nitrate
Crystalline structure

ABSTRACT

Crack openings in concrete lead to a reduction in its lifespan. Many authors have analysed different techniques that could repair cracks autonomously, being the use of bacteria one of the most promising approaches. Bacteria are often introduced with nutrients in the concrete mixes, and they may alter the cement hydration.

In this study, the effects that calcium lactate, calcium nitrate, and yeast extract have on cement pastes during the early hours of hydration were analysed. To accomplish this, calorimetry, in situ X-ray diffraction (XRD), Fourier Transform Infrared Spectroscopy (FTIR), Vicat and rheology techniques were employed. The results demonstrated that the addition of calcium lactate led to higher values of ettringite, which altered the rheological behaviour of the pastes. Moreover, when added at 4%, calcium lactate also delayed the setting time by inhibiting the reaction of silicates, a similar effect was observed when yeast extract was added. Lastly, the incorporation of nitrate accelerated the setting time.

1. Introduction and objectives

1.1. Introduction

Concrete is the most widely used construction material as it can be made with local resources, be adapted to different shapes, and achieve high compressive strength while maintaining a low production cost. However, its low tensile strength leads to the formation of cracks on its surface, exposing its matrix to harmful elements that can penetrate and damage the concrete or the steel rebars.

The repair of these cracks is usually limited to the largest visible ones employing techniques such as covering them with a new layer of mortar. However, this approach merely seals the surface externally without actually filling the crack [1]. Additionally, it is not uncommon for this process to entail numerous difficulties owing to the location or morphology of the structure resulting in an increase of the final cost of the maintenance [2]. A clear example is the repair of submerged or underground structures [3]. In addition, most of these repairs are only effective for 10 to 15 years, and 20% show defects after five years [4].

According to Mahmoodi *et al* [5], 50% of the annual construction budget in Europe is allocated to maintenance and repair projects. In the United Kingdom, these operations amount to a cost of 40 billion pounds a year [4]. In 2019, the British government committed to spending 500.000 million pounds during the years 2020 and 2021, trying to repair several infrastructures in the country, mainly made of concrete [4]. USA expended between US$300–400 million per year in the renovations of bridges and car parks alone in the late 2000s [6].

The combination of these factors has driven the research and development of new techniques that enable concrete to repair itself, also known as self-healing, to extend the useful life of structures and reduce the high maintenance costs. These processes can be classified as either autogenous or autonomous [7]. The first refers to the concrete's ability to repair itself owing to the hydration of cement particles that remain unreacted or to calcium hydroxide carbonation processes [8]. In contrast, autonomous self-healing refers to the repair processes induced by the incorporation of an external agent. These agents can be derived from electrodeposition technologies such as shape memory polymers [9], microcapsules [10], vascular technologies [11] or even microorganisms such as fungi or bacteria.

In the case of bacteria, the repair process occurs due to the precipitation of calcium carbonate induced by these microorganisms and their negatively charged cell walls. These cell membranes attract calcium cations that cluster on their surface, serving as nucleation sites and promoting their reaction with carbonates. In addition to crack sealing,

* Corresponding author.
E-mail addresses: adonay.pinto@udc.es (A. Pinto), bfonteboa@udc.es (B. González-Fonteboa), gumersinda.spaz@udc.es (S. Seara-Paz), fernando.martinez.abella@udc.es (F. Martínez-Abella).

https://doi.org/10.1016/j.conbuildmat.2023.133142
Received 27 January 2023; Received in revised form 23 August 2023; Accepted 24 August 2023
Available online 5 September 2023

the addition of these microorganisms and their nutrients impacts on other properties of the cement-based materials, enhancing values such as compressive strength [12], shrinkage [13], or water absorption [14].

Bacteria employed in self-healing concrete can be classified based on their metabolic path as ureolytic, denitrifying, and aerobic heterotrophic bacteria [15,16].

Ureolytic bacteria precipitate calcium carbonate due to urease, an enzyme produced by this type of bacteria capable of breaking down urea into ammonium and carbonate ions. This process facilitates the generation of a large amount of $CaCO_3$ [17]. However, for each carbonate ion generated, two ammonium ions are generated as well [18], resulting in nitrogen oxide emission into the atmosphere and an increase in armour corrosion [16]. As a result, this type of bacteria has raised some concerns, and many researchers avoid using it.

The bacteria that follow the second mentioned metabolic pathway, denitrifying bacteria, produce less calcium carbonate than other metabolic pathways [19], but they can function even in low-oxygen environments. As their name suggests, they use nitrate ions as alternative electron receptors in organic carbon oxidation, generating carbonate ions that react with calcium cations to form calcium carbonate.

Finally, heterotrophic aerobic bacteria convert organic compounds into carbonate ions, which are necessary for the self-healing process. In addition, carbon dioxide and water are generated during the decomposition process. These materials react with the calcium hydroxide present in the cracks, thereby improving the repair process [20].

Depending on the metabolic pathway followed by the type of bacteria employed, certain nutrients need to be incorporated into the mixture [17]. These nutrients, required either to enhance the survival of the bacteria or to improve the amount of calcium carbonate produced, are usually sources of carbon, nitrogen, and calcium salts to increase the number of calcium ions within the concrete.

In this regard, there is a wide variety of nutrients that can be employed in self-healing of cement based materials, including, for example peptone [21], calcium acetate [20], sodium citrate [22], calcium formate [23], and other calcium acid salts such as succinate, oxalate, malate, and glyoxylate [24].

The use of any of these nutrients entails a significant increase in the cost compared to other raw materials commonly used in cement-based mixes. Reducing the cost of this technology should be a priority with the aim of maintaining the price increase below 15-20€ per m^3 [22].

1.2. Objectives and research significance

The main hypothesis of this study is that nutrients, when they are not encapsulated, or the capsules break during the mixing or installation process, may induce changes in the behaviour of the cement-based materials in terms of their fresh and hardened properties. These changes, that have not been thoroughly investigated, might occur at early stages and in the fresh state.

According to the hypothesis established, the main objective of this research is the assessment of the hydration process and the rheological performance of the cement-based materials in the presence of different nutrients, especially at early ages. Moreover, there is a wide variety of nutrients and their quantity in the mixes moves in a large range. Both these issues make difficult to understand their effects on the performance of the cement-based materials. In addition, some previous research [25–30] investigate the effect of bacteria-nutrients systems in the cement hydration process, but they hardly focus on chemical changes that take place during the first hours of hydration.

In this study it was decided to study each nutrient separately, so that the changes that they generate can be clearly identified. The analysis is focused on the early age performance measuring calorimetry during the first 48 h and *in-situ* XRD to know the evolution of each crystalline phase. The rheological performance was also assessed using a continuous flow test for the first 60 min. These parameters have not been thoroughly analysed yet, and they are highly valuable in practical applications for understanding workability and field placement conditions.

Results about chemical changes at early ages due to the introduction of nutrients will help to identify the different hydration phases, to obtain their quantifications and to determine the time frames at which they occur. All of these will explain the rheological behaviour in the fresh state, which is crucial for understanding the workability aspects of cement-based materials during construction. Furthermore, the knowledge about chemical composition, will contribute to a better understanding of the self-healing process using microorganisms that require the inclusion of these specific nutrients.

The selected nutrients were yeast extract, calcium lactate, and calcium nitrate due to their high use in self-healing with bacteria, high availability and low cost. Yeast extract is a nutrient that provides nitrogen, vitamins, amino acids, and carbon [31]. Calcium lactate is a calcium salt that introduces calcium ions to the mixture [32], improving the precipitation of calcium carbonate [32] which is the main component of the self-healing process [33]. Calcium nitrate is another calcium salt mainly used along with denitrifying bacteria, as well as with other types of bacteria [34–36], as it enriches the mixture with calcium ions.

2. Materials and methods

2.1. Materials and cement pastes

Commercial CEM I 52.5 SR-5 ordinary Portland cement was used in this study. Its chemical composition, measured by X-ray fluorescence, is presented in Table 1. Loss of ignition (LOI) was also measured. Its mineralogical composition, identified by X-ray diffraction and quantified by Rietveld refinement, includes alite (67.3%), belite (6.9%), C_3A (2.5 %), C_4AF (12.7 %), gypsum (4.7 %), calcite (3.8%), arcanite (2.0 %), and traces of anhydrite, bassanite, and syngenite.

A commercial limestone filler (LF), the chemical composition of which is listed in Table 1, was used. Mineralogically, the filler consists mainly of calcite (97.1%), although it also contains minor amounts of dolomite (1.3%) and quartz (1.6%).

The water used was local tap water. The filler/cement ratio and water/cement ratio in the control cement paste were 0.43 and 0.5, respectively.

The nutrients chosen for the test were yeast extract, as a base nutrient for the growth of bacteria, and calcium lactate and calcium nitrate to provide the extra amount of calcium required to obtain Microbially Induced calcium carbonate precipitation (MICP). The percentages chosen for their study were selected based on previous trials and information obtained from the literature [12,35,37–42]. The designation of each paste, representing the concentrations of nutrients relative to the cement mass (in percentage), followed by the initial letters of the corresponding nutrient, is listed in Table 2.

Table 1
Chemical composition of CEM I and limestone filler used.

	CEM I 52.5 SR-5	LF
CaO	61.8	55.0
SiO_2	18.5	1.5
Al_2O_3	4.6	0.5
Fe_2O_3	3.7	0.2
SO_3	3.1	0.2
MgO	1.7	0.5
K_2O	1.0	0.1
TiO_2	0.2	–
MnO	0.1	–
P_2O_5	0.1	–
LOI		41.9

Table 2
Nutrient content per paste measured by % over cement by mass.

Paste	Nutrient	Nutrient content (% over cement by mass)
REF	–	–
1LAC	Lactate	1
4LAC	Lactate	4
2NIT	Nitrate	2
2NIT1LAC	Nitrate	2
	Lactate	1
0.75YE	Yeast extract	0.75

2.2. Methodology

2.2.1. Isothermal calorimetry

A TAM Air 8-channel isothermal calorimeter was utilized ~~to~~ for measuring the heat flow in the pastes and to assess the kinetics of hydration of the different mixes. We chose water as the reference material, and the heat capacity of each sample was matched to each reference.

The accessory for internal mixing, Admix Ampoule, was used for analysing the first 45 min of hydration. In this case, the powder was placed inside the glass ampoule, and the liquid phase was introduced throughout the syringes to avoid mixing before the calorimeter was ready.

The nutrients were dissolved and introduced with the corresponding mixing water in the syringes. The mixing process of the paste lasted for 1 min 30 s.

The heat flow curve up to 48 h was measured by applying an external stirring method. This guarantees better mixing and higher repeatability of the results compared to internal mixing [43]. The mixing time of 1 min and 30 s was chosen trying to minimize the elapsed time between water-cement contact and the beginning of the tests, while ensuring the homogeneity of the mixture. The first 30 s were used to homogenize the powder materials, mixing the limestone filler and the cement together in dry conditions. After that, the wet mixing process (powder material plus water with nutrients dissolved) starts, lasting 60 s. This is a common time used by other researchers [44–46]. This process ensures a uniform blend without enlarging the period between the powder – water contact and the initial testing too much. When the mixing process was complete, the pastes were transferred into plastic ampoules and inserted into the calorimeter.

Both procedures were performed using a calorimeter set to 25 °C, and the signal was normalised according to the cement mass.

Two samples were tested for each paste.

2.2.2. In-situ X-ray diffraction and Rietveld refinement

The phase development during paste hydration was examined during the first 48 h using in situ XRD. The mixing process used was the same employed in the calorimetry external stirring method, mixing the cement and limestone filler by 30 s, then adding the water with the nutrient dissolved, and mixing again for 60 s. After mixing, the sample was covered with a 7.5 μm thick Kapton ® polyimide film to avoid water evaporation and finally placed inside the D4 Endevour diffractometer by Bruker. A step width of 0.035 ° with 1.3 s/step was employed to map the region from 7° to 40° 2θ, resulting in a measurement roughly every 20 min during the first 24 h. After that, the conditions were changed to 0.035° and 3.9 s/step to gain accuracy and measurements were taken for the next 24 h. It is worth noting that, one of the limitations of using in situ XRD lies in the trade-off between covering a wide range of diffraction angles within a limited time frame and maintaining a good signal–noise balance in the measurements.

A total of 88 diffractograms were taken for each sample. The diffraction patterns were then refined using the open-source software PROFEX [47] and the external standard method [48–50] to obtain the composition of the paste in term of % of crystalline phases. Anhydrous cement data were used as the starting point for refinement and the standard material used was Corundum 674a from Nist.

By combining the data from both calorimetric measurements and XRD quantification, a comprehensive understanding of the hydration process and its physical changes can be achieved, providing valuable insights into the chemical reactions and kinetics of the cementitious materials [44,48,51].

2.2.3. Setting time

The setting time was measured using an automatic Vicat device following the UNE-EN 480-2:2006 standard. This time was used to know the time required to set and harden the cement mix which is related to phase formation.

To perform this test, a conical mould of the dimensions set by the regulations was filled and inserted into the Vicat apparatus. The apparatus has a previously calibrated needle that falls freely and enters the paste. The start of the setting time was confirmed when the needle could no longer reach the bottom and stopped 4 mm from it. The final setting time was measured when the needle could only be inserted 2.5 mm from the surface. The mixing method was the same as the one used for the rheological tests (Fig. 1).

2.2.4. Rheology

Rheological performance is an important issue directly linked to the workability of the cement-based materials. To examine the influence of nutrients on the rheological properties of the paste, a continuous flow test for 60 min and a Flow Curve Test (FCT) were carried out in separate batches. Both rheological tests were performed at 25 °C in a Viskomat NT rheometer equipped with a fishbone probe. The measurement setup consists in a stationary paddle positioned at the centre of a rotating cylindrical container. The movement of the sample around the stationary paddle produces a consistent torque, which is recorded. The powder materials were mixed by placing them in a 1-liter mixer for 30 s and then, water with dissolved nutrients was added and mixed for another minute. After mixing, the sample was placed in the rheometer to perform the continuous flow test. The test involves inserting the probe into the paste and hold still. Following that, the rotation began at 6 rpm until the 60 min mark was reached.

In the FCT, the sample was placed in the container immediately after mixing. Then, the mixture was accelerated over the next 5 s of the test until it reached the target speed of 168 rpm, which was maintained for another 30 s. Subsequently, 7 steps of 10 s each were performed, during which the speed gradually decreased until it reached 0 rpm after the final step. To determine the dynamic yield stress and plastic viscosity, the Bingham fitting model was applied using Equation 1 [52–54].

$$\tau = \tau_0 + \mu\gamma \quad (1)$$

where τ is the shear stress (Pa), τ_0 is the dynamic yield stress (Pa), μ is the plastic viscosity (Pa·s), and γ is the shear rate (1/s). This test was also performed 10 min and 1 h after the contact of cement and water, but the results for some of the samples exceeded the machine reading limit. Therefore, only the results of the initial measurement are shown.

Fig. 1 shows the mixing procedure and test protocol.

2.2.5. Fourier transform infrared spectroscopy (FTIR)

Fourier-transform infrared technique is a spectroscopy method used to characterize composition of cementitious materials in combination with other methodologies as XRD. Infrared spectroscopy was utilised with 4LAC and 0.75YE to elucidate some results seen in the rheological and X-ray diffraction test. These pastes were prepared using the same procedure described for the external stirring method in the calorimetry section.

The hydration process was stopped at 15 min and 4 h, and the paste was dried using the solvent exchange method. In this method, the water of the sample was replaced by a solvent, and then the solvent was removed by ambient or vacuum drying [55]. After 24 h in acetone, the 4 h samples were subjected to vacuum drying at 40 mBar for 1 h. The

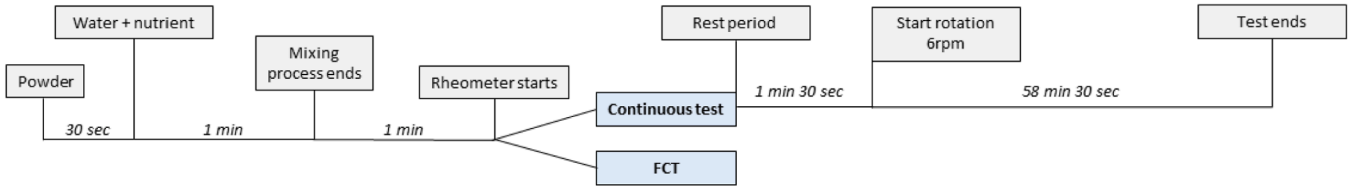

Fig. 1. Mixing procedure and protocol for the rheological tests.

samples that were hydrated for 15 min, were immersed in acetone for 30 min and then dried at 60 °C on a conventional stove. Both samples were ground into fine powders to perform the test. Measurements were taken in the range of 400–4000 cm^1.

3. Results and analysis

3.1. Isothermal calorimetry

The isothermal calorimetry results are shown in Fig. 2, which shows the evolution of the heat flow in the pastes during the first 48 h.

The reference (REF) mix exhibited the behaviour of a conventional cement paste during hydration. After the initial heat release, a period of minimal activity, associated with the induction period, started. Following that period, the hydration heat increased abruptly due to silicate hydration and the growth of calcium silicate hydrate (C-S-H). This acceleration phase extended until the maximum (1st peak) was reached, at approximately 6.4 h for the REF mix, indicating the beginning of the deceleration period. Following the start of this deceleration phase, the increase in the C3A reaction caused by the consumption of sulphates, which usually results either in the rapid precipitation of additional ettringite or in the formation of AFm phases, was marked by the formation of a smaller peak (2nd peak). This "shoulder" appeared 9.5 h after hydration started in the REF paste. After this, the decline in the heat flow continued undisturbed until approximately 22 h, when another slight shoulder was observed (3rd peak). This lasted nearly 40 h and was associated with the formation of hydrated calcium monocarbonate and the AFm phase in general due to ettringite destabilisation [56].

All pastes reflected the same behaviour as REF in terms of periods: pre-induction, induction, acceleration, and deceleration were visible for the six pastes analysed. However, adding nutrients altered the length and shape and even eliminated some peaks.

Regarding the addition of calcium nitrate, the 2NIT paste showed a calorimetric curve that was almost superimposable on that of the REF paste during the acceleration phase, with only a slight decrease in the duration of the induction period and a slight decrease in intensity and time at the maximum. This was consistent with the accelerating properties of calcium nitrate. The intensity of the "sulphate depletion" peak of the 2NIT heat flow curve decreased, and there appeared to be no 3rd peak at the end of the curve.

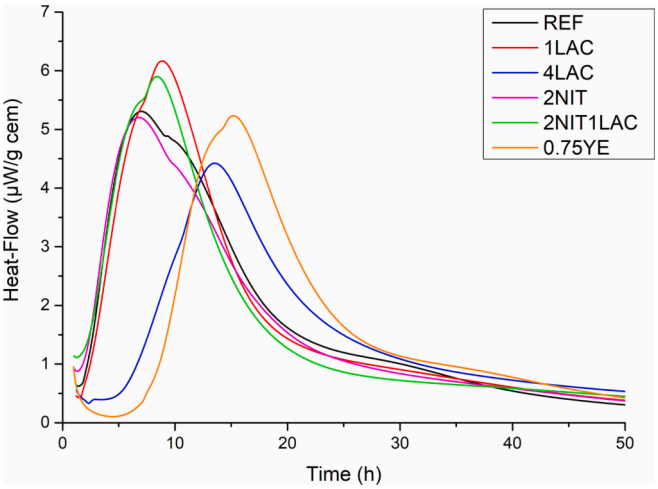

Fig. 2. Heat-flow evolution during the first 48 h of hydration

The addition of calcium lactate slowed the reaction of C_3S, resulting in a smaller slope owing to the retardation of cement hydration by some hydroxycarboxylic acid salts [57]. Although the curve for 1LAC was less steep than for the REF, adding lactate at 1% did not significantly modify the behaviour of the acceleration paste. 1LAC and REF mainly differed in terms of their maximum and the 2nd peak. The silicate reaction appeared to terminate almost at the same level in both curves. However, instead of starting the deceleration period, 1LAC kept increasing its heat flow values until 6.16 μW/g-cement and then began to decline without showing that 2nd characteristic peak for the sulphate depletion. The 3rd peak was also not visible in this paste.

The addition of 4% calcium lactate, also modified the behaviour. The induction period was extended from 1 h (REF and 1LAC mix) to 3.5 h. The slope of the acceleration phase is even lower than that of 1LAC. Additionally, it reached a considerably lower maximum at 4.4 μW/g cement at 13.5 h without any distinguishable variation in the slope. This made it difficult to identify the end of the reaction of the silicates or whether there was also formation of AFm phases at that point. During the deceleration period, no 2nd or 3rd peak was observed.

The combined addition of calcium lactate at 1% and calcium nitrate at 2% (2NIT1LAC) showed a calorimetric curve similar to that of 1LAC, as expected considering the low effect observed on the 2NIT heat flow curve. 2NIT1LAC also had an acceleration period that did not end at the 1st peak. As in 1LAC, after an inflection point, the heat flow continued increasing until it reached a new maximum that was slightly lower than that achieved with 1LAC. There were no signs of the sulphate depletion "shoulder" after this 2nd peak, nor was there a 3rd peak.

Finally, the addition of yeast extract caused a partially inhibited reactivity. As a result, there was a delay and decrease in the general intensity of the calorimetric curve compared to the REF mix, particularly regarding the induction period extending past 7 h of hydration. Yeast extract is rich in carbohydrates, which are known for their retarding effect on silicate reactions [58]. The maximum reached after the acceleration period is quite similar to that of the control paste. Following that, the curve presented the same shape as the ones observed for samples with 1% lactate. In this case, there was no excess ettringite that could be destabilised to form AFm-type phases. Additionally, although there is no 2nd peak visible in the deceleration period, a small perturbation where the 3rd peak should be, was observed. This indicates that the peak reached at the end of the acceleration phase has a different underlying source from those of 1LAC and 2NIT1LAC.

The heat flow measured during the first few minutes of hydration using the internal stirring method, is shown in Fig. 3. This figure depicts the initial peak recorded at the beginning of hydration, which is characterised by a rapid exothermic reaction. This reaction is usually related to the dissolution of mineral phases that liberate calcium ions into the solution, the reaction of C3A with gypsum and other sulphates, the formation of ettringite, and lastly, the formation of a small C-S-H gel as a

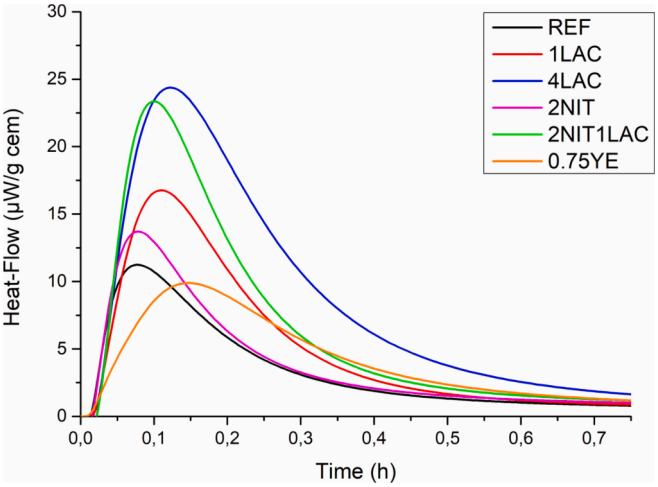

Fig. 3. Heat-flow evolution during the first minutes of hydration measured by the internal stirring method.

protective layer that causes the induction period [59].

The addition of nitrate did not have a significant effect compared to the control. This lack of variation was also reported by Dorn *et al.* [60].

With the addition of lactate at 1% (1LAC), the initial heat-flow rose by 50% compared to REF. However, when the two calcium salts were added (2NIT1LAC), the initial peak was higher than that of both nutrients separately. Moreover, as in the case of the acceleration period, the 2NIT1LAC curve was more similar to that of 1LAC than to that of 2NIT in terms of the peak location. For 2NIT, there was no time increase, and it reached the maximum almost at the same time as the REF.

The maximum increase in heat flow was observed in 4LAC, where the peak was almost 150% higher than that of the REF mix.

Yeast extract is the only nutrient inhibiting this phase. The calcium nitrate and lactate used in the other pastes promoted the dissolution and reaction of the aluminates, increasing the intensity of the initial heat flow compared to the REF mix. The peak reached by 0.75YE was 12% lower than the one reached by the REF paste, which took twice as long.

3.2. *In situ* XRD and Rietveld refinement

3.2.1. *Effect of calcium lactate*

Fig. 4 compares the behaviour of REF paste to those containing calcium lactate as a nutrient. Regarding the phases related to the silicate reaction (alite and portlandite), the initial alite content in REF paste was slightly lower than the theoretical value for the anhydrous mixture (34.3%) and remained approximately constant for up to 2 h. Thereafter, alite was quickly consumed, and at the same time, portlandite formation became detectable. Both processes proceeded simultaneously until they stabilised after about 17 h of hydration. This process was consistent with the acceleration period shown in the calorimetric curve, in which the induction period ended shortly before the alite reaction became evident, and where the maximum, signifying the end of the acceleration period, was observed approximately at the inflection point of the curves defining the consumption and formation of alite and portlandite.

The addition of 1% lactate resulted in an alite consumption rate resembling that of REF paste during the first 5 h of hydration. However, the behaviour of the 1LAC paste beyond that point differed from that of REF, with faster dissolution of the alite being observed in the former. This is in agreement with the calorimetric curves, as the REF heat flow curve stabilised quickly after 5 h to give rise to the maximum acceleration period. In contrast, the 1LAC curve required more time to reach this stabilisation, exhibiting a greater slope up to approximately 7 h. Although alite consumption was promoted in the 1LAC paste after 5 h of hydration, once it stabilised, the achieved values of undissolved alite were only slightly lower than those observed in the REF paste.

Regarding the 4LAC paste, no alite consumption was observed until 4–5 h of reaction, as expected, considering that the induction period displayed in the calorimetric curve was extended until approximately this point. Following this, the curve defining the dissolution of alite evolved in parallel to that corresponding to 1LAC, tending to stabilise with alite concentrations higher than those of 1LAC and REF pastes.

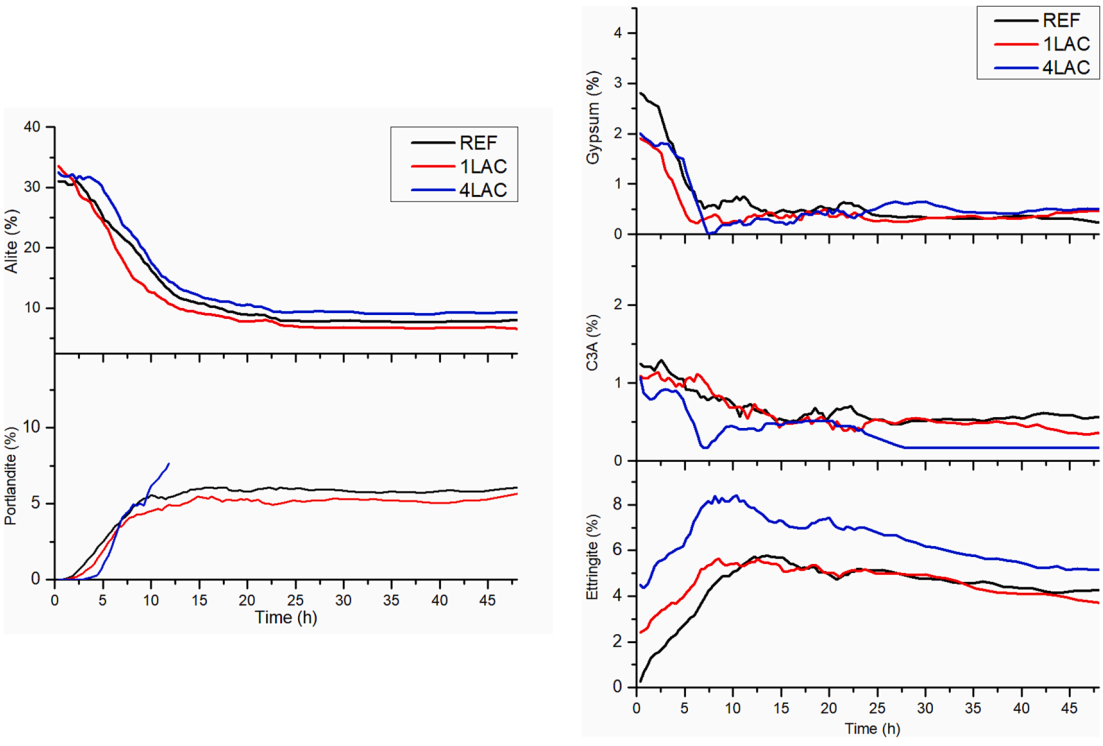

Fig. 4. Evolution of the different crystalline phases analysed in the pastes containing just lactate.

The evolution of the portlandite curve qualitatively agreed with the behaviour observed for alite in pastes containing calcium lactate, meaning that the onset of its precipitation coincided with the initiation of the alite reaction and that they stabilised synchronously. However, there were significant quantitative discrepancies with the expected values, particularly after 5 h of reaction. At this point, neither the increased amounts of portlandite anticipated from the acceleration of the silicate reaction in 1LAC nor those reduced by its inhibition in 4LAC were detected. This was attributed to the strong preferential orientation of portlandite observed in the XRD tests. This common phenomenon occurs during in-situ XRD tests, where the growth of a small number of large portlandite crystals may be observed [46,61]. Consequently, the diffractograms displayed an excessive intensity of the peak corresponding to the (0 0 1) plane of portlandite, which greatly hindered adequate quantification. This effect was particularly exaggerated in the 4LAC sample, especially after 10 h. Therefore, no results corresponding to longer reaction times are shown in Fig. 4.

As for the aluminate reaction, the REF paste exhibited an initial C_3A value slightly below the theoretical value at zero hydration time (1.3%), which gradually decreased over a period of approximately 15 h. At this stage, C_3A could be considered to be totally consumed, given the inherent error in the quantification method. Ettringite precipitated synchronously, reaching a maximum at 15 h, coinciding with the total consumption of C_3A. The maximum value of ettringite reached is approximately 6%, matching the theoretically achievable amount of ettringite resulting from complete C_3A dissolution. In parallel, gypsum dissolution occurred during the first 5 h of the reaction. Ettringite formation is expected to continue after gypsum consumption, as the total consumption of the sulphate ions in the solution tends to cause desorption of the sulphate ions located on the surface of C_3A particles to restore chemical equilibrium. This leads to a sudden increase in the ettringite formation, which is one of the most common causes for the development of the sulphate depletion peak in the heat flow curves. In this case, the sulphate depletion peak appeared at approximately 10 h, that is, at the same time as the extra precipitation of ettringite takes place [62]. Additionally, no initial gypsum consumption was observed, and gypsum levels at the beginning of the reaction were even higher than the theoretical values for a zero reaction rate (2.4%). Gypsum was not the only source of sulphates in the system since there was a substantial amount of arcanite in the starting cement, as described in Section 2.1. As arcanite is easily dissolved, especially compared to gypsum, it was the primary source of sulphate ions at the beginning of the reaction. As seen in this case, excess calcium in the system could easily lead to the precipitation of additional gypsum. Finally, the concentration of ettringite slowly decreased after 15 h. This can possibly be attributed to its destabilisation due to the scarcity of sulphates in the solution and the subsequent formation of AFm phases. These phases are typically in the form of monosulphoaluminates, given that they present a lower sulphate-to-alumina ratio than ettringite. However, AFm phases were not detected by XRD, which is common due to the low crystalline character of this type of compounds.

The addition of calcium lactate had an important impact on the aluminate reaction. Both the 1LAC and 4LAC pastes exhibited a higher initial consumption of gypsum and C_3A compared to the REF paste, which also resulted in increased ettringite precipitation at the beginning of the reaction. This effect was more prominent in the 4LAC paste, which exhibited a two-fold increase in ettringite content in the early stages of the reaction compared to the 1LAC paste. Such an initial enhancement of the aluminate reaction could account for the differences observed in the pre-induction period of the calorimetric curves in Fig. 3, in which the associated cumulative heat is approximately twice as high at 4LAC compared to 1LAC. Regardless of the differences observed at the beginning of the reaction, the ettringite formation in the 1LAC and 4LAC pastes progressed according to that observed in the REF paste. Nevertheless, the maximum concentration was reached earlier than in the REF paste, at approximately 8 h in both cases. This period corresponded to the gypsum consumption time, which is the limiting factor in ettringite formation. This suggests that lactate inhibited the adsorption of sulphate ions on the surface of C3A particles. The maxima observed near 9 and 13 h for the heat flow curves of the 1LAC and 4LAC pastes, respectively, did not correspond to the typical sulphate depletion peak caused by the desorption of sulphate ions into the solution, given that these peaks are not accompanied by an increase in ettringite concentration. These peaks likely originated from the destabilisation of ettringite and the formation of AFm phases. Furthermore, the calorimetric curves of the pastes containing calcium lactate did not exhibit the typical broad maximum of AFm phase formation towards the end of the deceleration period that was observed in the control paste at 25 h. This supports the idea of the development of this type of compound at earlier ages.

The maximum amount of ettringite produced was another factor to consider regarding the influence of calcium lactate on the aluminate reaction. The addition of 1% calcium lactate had no significant effect on the amount of ettringite formed, but on its precipitation rate. However, its use at concentrations of 4% enhanced this acceleration and promoted the development of larger amounts of ettringite. Additionally, the highest ettringite content in 4LAC amounts to nearly 8%, which was approximately 30% higher than the theoretical quantity achievable from the complete dissolution of C_3A, indicating that the dissolution of ferrite is also being promoted. This might be attributed to the ability of lactate ions to form metal complexes. Its hydroxyl and carboxyl groups enable lactate to behave as a chelating ligand capable of forming stable coordination compounds in solution with metal ions such as Al^{3+} and Fe^{3+} [63–65]. Consequently, lactate could facilitate the dissolution of phases such as C_3A and ferrite, thus enhancing the aluminate reaction. However, the stability of these coordination compounds in the complex pore dissolution environment of cement-based materials is uncertain, and further studies are required.

3.2.2. *Effect of calcium nitrate*

The evolution of the crystalline phases during hydration in nitrate-containing pastes is shown in Fig. 5. Although calcium nitrate is known for its accelerating properties, the alite consumption in the 2NIT paste did not show a clear trend of acceleration compared to the REF paste. During the first 9 h of hydration, the reaction of the silicates was distinctly slowed down, exhibiting lower rates of alite dissolution and portlandite precipitation than the REF paste. This is in agreement with the form of the 2NIT calorimetric curve during the acceleration period. Despite starting earlier than that of REF, the curve exhibited a slightly lower slope and stabilises at a less intense and slightly earlier acceleration maximum. However, the trend changed after 9 h, when the rate of alite consumption started to increase, and the amount of portlandite precipitated exceeded that of the REF paste.

The simultaneous addition of calcium nitrate and calcium lactate did not have a combined effect compared to the reaction of silicates. The alite consumption curve was virtually identical to that observed for the 1LAC sample. Thus, it exhibited similar behaviour to that of the REF paste during the first 5 h, followed by an acceleration of the alite dissolution relative to the REF paste. The portlandite formation curve likewise showed this acceleration of the silicate reaction after 5 h of hydration.

In contrast, the addition of calcium nitrate significantly influenced the evolution of the remaining phases. First, the initial amount of gypsum in the 2NIT paste was above the theoretically expected initial concentration and substantially higher than the amounts found in other pastes. As explained in the previous section, the presence of readily soluble arcanite might cause additional gypsum precipitation, as observed in the REF paste. The highly soluble calcium nitrate provides an additional supply of calcium ions into the solution at the start of the hydration process. This further facilitates the saturation of the solution with respect to gypsum and its subsequent precipitation by dissolving in conjunction with the arcanite. This was not observed in the 2NIT1LAC paste, even though calcium lactate served as an additional calcium

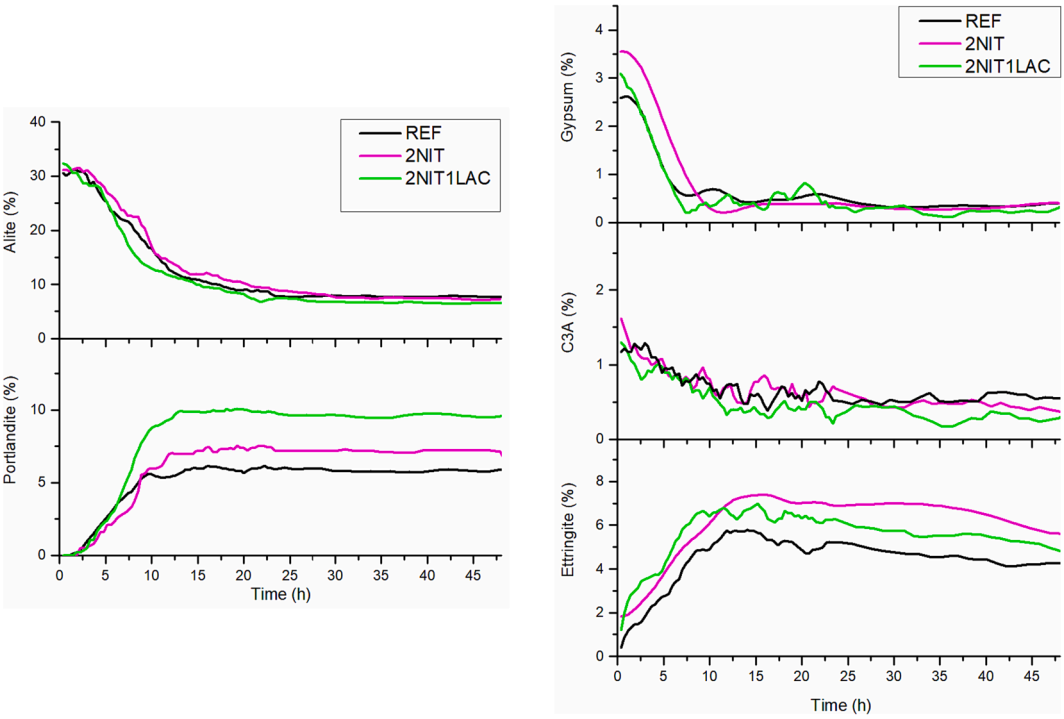

Fig. 5. Evolution of the different crystalline phases analysed in the paste containing calcium nitrate.

supply in this paste. This is explained by the fact that the reaction of the aluminates is promoted in the 2NIT1LAC paste, as seen in the calorimetry and confirmed by the initial quantities of ettringite observed in Fig. 5, which were similar to those of 1LAC. Under these circumstances, the additional calcium provided by $Ca(NO_3)_2$ was largely destined to end up in the precipitation of ettringite, which is less soluble than gypsum.

Another possible consequence of secondary gypsum precipitation in the 2NIT paste could be the decrease in the hydration acceleration capacity of calcium nitrate. The accelerating properties of $Ca(NO_3)_2$ are often attributed to its ability to increase the saturation of the solution compared to portlandite, thereby favouring its crystallisation [60,66]. Therefore, if the extra calcium ions provided by calcium nitrate result in gypsum precipitation, the acceleration effect is likely to be reduced. This viewpoint is supported by the fact that the accelerating effect of nitrate is not clearly observed in the XRD results until gypsum is consumed, at which point an increase in portlandite production was immediately visible.

The development of the ettringite formation was also sensitive to the addition of calcium nitrate. The progression of the 2NIT paste was similar to that of the REF paste, with a gradual increase in ettringite concentration up to approximately 15 h, when the ettringite started to destabilise. Ettringite precipitation in the REF paste continued beyond the total gypsum consumption, which took place after approximately 8 h of reaction. As a result, the sulphate depletion peak was attributed to the ettringite formation caused by the desorption of sulphate ions on other particles (e.g., C3A). The main difference in ettringite formation between the REF and 2NIT pastes was its concentration, which was substantially higher in the 2NIT paste. This might result from the extra calcium ions supplied by calcium nitrate, which facilitate the saturation of the solution with respect to ettringite, whose saturation index is highly determined by the concentration of calcium in the solution [67]. Conversely, the 2NIT1LAC paste showed a behaviour closer to that of 1LAC, where the maximum amount of ettringite was reached at the moment of total gypsum consumption (approximately 8 h). Therefore, the sulphate depletion peak was also related to the formation of AFm phases, as observed for 1LAC. However, as illustrated in Fig. 2, the intensity of the sulphate depletion peak was considerably lower in the 2NIT1LAC paste than in the 1LAC paste. This could be attributed to the fact that in the current situation of high availability of nitrate ions in the solution, nitroaluminate-type AFm phases can easily form, which exhibit a less negative formation enthalpy than other AFm phases such as sulphoaluminates or carboaluminates [68,69]. Finally, the maximum amount of ettringite reached in 2NIT1LAC was relatively higher than that in 1LAC, possibly because of the effect of the calcium ions of $Ca(NO_3)_2$ on the saturation of the solution.

3.2.3. *Effect of yeast extract*

Fig. 6 compares the quantitative XRD analysis of REF and 0.75YE pastes. It was evident that yeast extract inhibited the silicate reaction. First, this was apparent by the delay in the start of the alite reaction and the concomitant formation of portlandite. The latter occurred after approximately 8 h of reaction time and coincided with the end of the induction period in the calorimetric curve. Second, the maximum reaction rate point, which was easily distinguishable in the portlandite precipitation curve, was shifted to about 12 h, matching the maximum acceleration peak. In addition, yeast extract reduced the degree of hydration attained, as the alite dissolution tends to stabilise at higher concentration levels than the REF paste. Consequently, the precipitated portlandite declined to lower levels.

The reaction of the aluminates was also suppressed. Gypsum dissolution slowed down, and gypsum was not being consumed until 6 h of reaction time. However, the formation of ettringite was observed at this stage, which probably resulted from the sulphate ions provided by the dissolution of the arcanite derived from the anhydrous cement. Once gypsum was depleted, ettringite precipitation accelerated. This occurred significantly before the sulphate depletion peak of the calorimetric curve, suggesting the existence of another source of sulphate ions.

Yeast extract is a multi-component mixture comprising several organic compounds. Therefore, a complex effect on cement hydration is expected when it is added as a nutrient. Although it is difficult to draw definitive conclusions given its intricate composition, carbohydrates are key ingredients in yeast extract and are known to delay cement hydration [58,70]. Although the effect of carbohydrates is usually associated

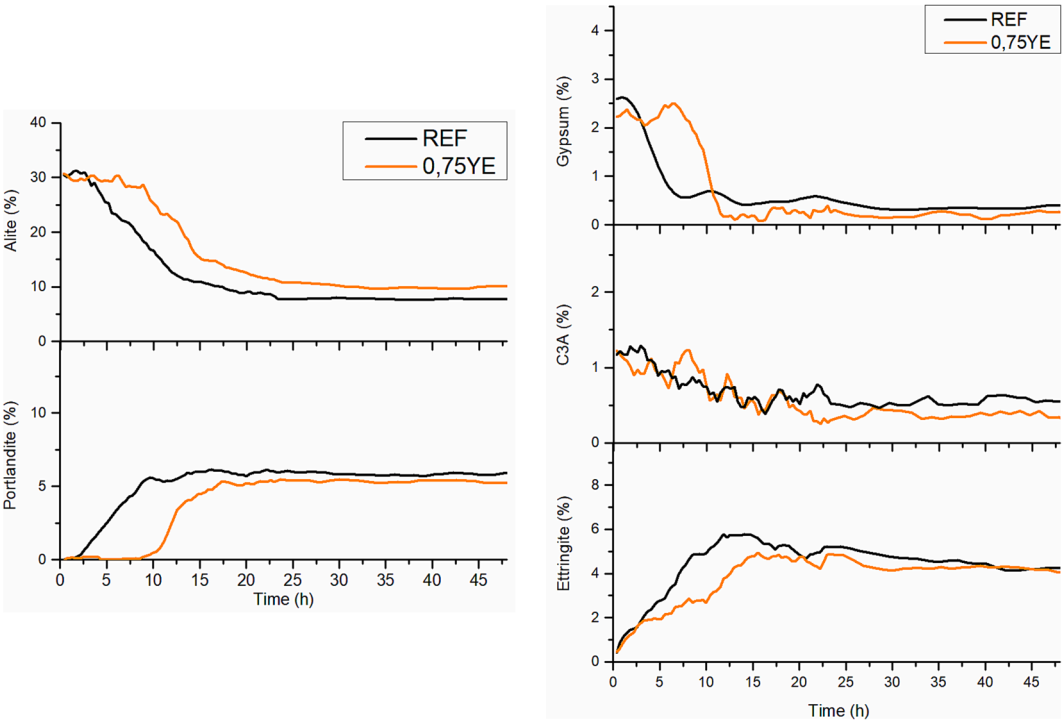

Fig. 6. Evolution of the different crystalline phases analysed in the paste made with yeast extract.

with the reaction of silicates, sugars, such as glucose, have also been reported to inhibit gypsum dissolution and ettringite formation [71,72].

3.3. Setting time in vicat test

The (Fig. 7) shows the setting time results of all mixes. Calcium nitrate acts as a setting accelerator when used with low-tricalcium aluminate cement [73] such as the cement used in this study. The addition of 2% of this salt combined with 1% of lactate (2NIT1LAC) reduced the initial setting time by 5%, while the final setting time was reduced by 15.5% compared to the REF mix. This effect in the final setting time was preserved when the nitrate was introduced alone (2NIT), showing a reduction of 14.5% when compared to the REF mix. However the initial setting time is lower in the 2NIT than in 2NIT1LAC, showing a reduction of almost 18% when compared to the REF mix, which makes it to present the fastest setting. These results are in agreement with those presented in section 3.2.2, showing that the alite consumption and portlandite precipitation were reduced during the first hours of 2NIT. This was due to the presence of secondary gypsum, while the additional calcium in 2NIT1LAC made the mixture behave more like 1LAC than 2NIT. The presence of secondary gypsum is the only explanation we can deduct from the chemical analysis results, that can justify the results of the initial setting time as was also stated by other authors [74,75]. In further research we will try to confirm this secondary

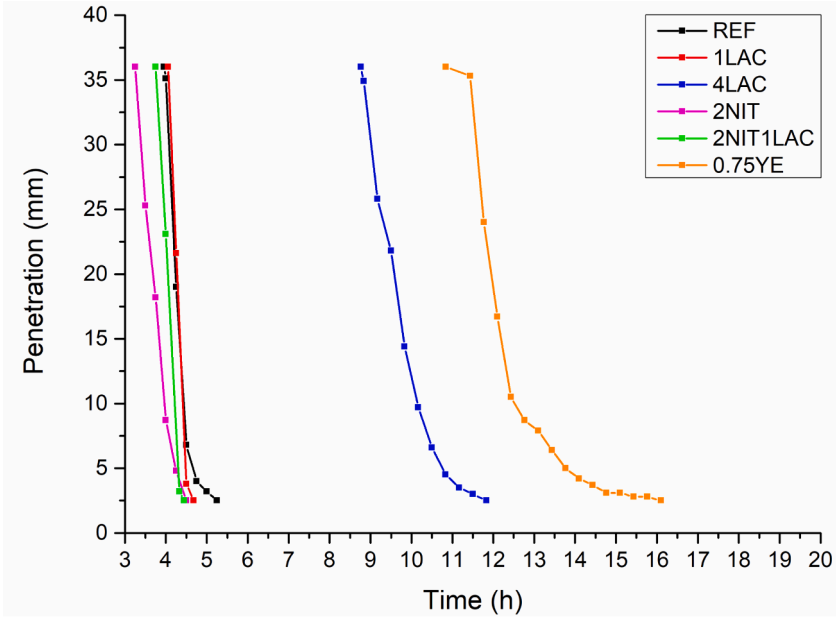

Fig. 7. Setting time results measured by an automatic Vicat device.

gypsum with SEM images.

When 1% calcium lactate was added alone (1LAC), the initial setting time remained unaffected, and both the REF mix and the 1LAC mix started setting at approximately 4 h. However, the final time in 1LAC was reduced compared to the REF mix by 11%.

The 4LAC and 0.75YE mixtures generated the most significant change in terms of setting time. Yeast extract composition based on amino acids and carbohydrates inhibited alite consumption, delaying the setting's beginning and end by 174% and 206.5%, respectively. On the other hand, the delay for 4LAC corresponded to an increase of 122% in the initial setting time and 126% in the final setting time.

As demonstrated in Section 3.2.1, adding 4% calcium lactate to the mix inhibited the consumption of the alite phase during the first hours of hydration, resulting in a longer induction period, as observed in the calorimetry curve (Fig. 2). This delay in the hydration process was attributed to the effect of alpha-hydroxy acids, such as calcium lactate, that were generated during the cement hydration processes.

3.4. Rheology

3.4.1. Continuous flow test

Fig. 8 shows the evolution of torque during the first 60 min after hydration. The curve corresponding to the REF paste was characterised by a rapid initial increase in torque until it reached a maximum, followed by a rapid decrease from the peak (in a few seconds), and a slow, asymptotic decrease. This is the typical behaviour for this type of material, in which the application of shear force causes an increase in torque until the start of the fluid movement is reached, due to the thixotropy of the mixture and the destructuring forces exerted on it. This behaviour was also observed in the 2NIT paste, but with slightly higher torque values in the first few minutes. The formation of secondary gypsum in 2NIT, observed in the XRD results, might have caused the loss of workability in this mixture due to the loss of available water in the solution and the interlocking of the formed gypsum crystals [76–79].

The pastes containing 1% lactate (1LAC and 2NIT1LAC) exhibited a considerably higher value of the maximum peak associated with the start of the fluid movement, reaching a value of about 3 times higher than that of the REF paste. Subsequently, the torque decreased in a few seconds, similar to that of the REF mix. The behaviour in the subsequent destructuring phase differed from that of the control mix, in two distinct stages: i) an initial slow decline in torque that stabilised at approximately 20 min and ii) a second stage in which torque decreased at higher speed reaching the equilibrium at approximately 40 min. This behaviour could be attributed to the amount of ettringite formed during the first few minutes of hydration, as discussed in the previous section. This extra ettringite reduced the amount of available water in the mixture, increasing the measured torque in 1LAC and 2NIT1LAC.

The other two pastes, 4LAC and 0.75YE, behaved differently from the previous pastes. At the beginning of the test, both exhibited an initial peak considerably lower than the others (1LAC and 2NIT1LAC). The peak in the 4LAC mix was higher than that in REF, while 0.75YE exhibited the opposite. The torque then decreased for a few seconds, followed by a stage where it increased again (this period lasted up to 10 min). At this stage, the peak reached was similar to the first peak and was maintained for up to 20 min. Subsequently, a new stage of gradual decline in torque was observed.

The results suggested that one or several processes during the hydration of the pastes favoured their structuring during the first 20 min, reaching the point of exceeding the shear stress applied to the 4LAC and 0.75YE pastes in certain phases of the experiment. Given the stage at which these processes occur, it was reasonable to attribute the observed increases in torque to the formation/reaction of products related to aluminates and/or sulphates. Since the compositions of both pastes were different and this behaviour change could not be explained by the XRD results presented in Sections 3.2.1 and 3.2.3, we decided to employ Fourier transform infrared spectroscopy at 15 min and 4 h of hydration for both mixtures.

3.4.2. Flow curve test

The results of the Flow Curve Test (FCT) are shown in Fig. 9, where the dynamic yield stress and viscosity of the mixtures, immediately after the mixing process, are displayed.

The results agreed with those from the continuous flow test. The mix with 2NIT had increased viscosity and yield stress compared to the REF mix. Additionally, the viscosity was the parameter affected to a greater extent, increasing by 34%.

Similarly, using lactate at low percentages (mix 1LAC and 2NIT1LAC) caused an increase in the rheological parameters. However, when calcium lactate was employed in a high amount (4LAC), the viscosity and the yield stress significantly decreased by 43% and 52%, respectively. Calcium lactate particles tend to adhere to cement particles, causing a repulsion effect that reduces the viscosity and yield stress [80]. In 1LAC, the amount of lactate added to the mix was not sufficient to generate the same repulsion forces among particles that 4LAC had, and the effects of lactate produced in the reactions of aluminates prevailed. Finally, the use of yeast extract (0.75YE) also reduced both rheological parameters, but to a lesser extent, 4% for the viscosity and 38% for the yield stress.

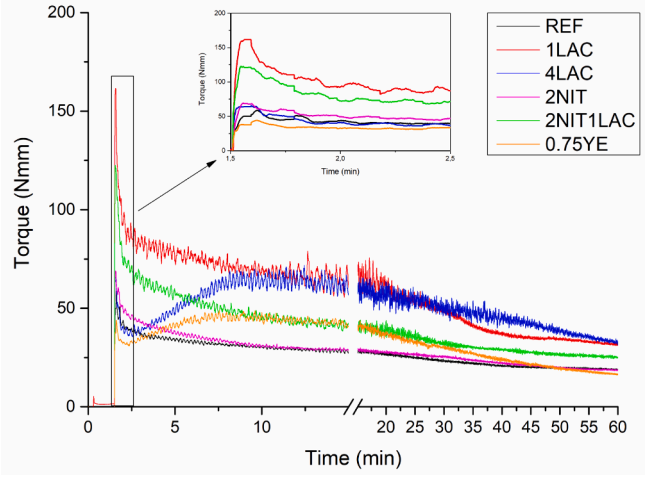

Fig. 8. Torque obtained in the continuous rheological test after a resting period of 1.5 min (3.5 min age).

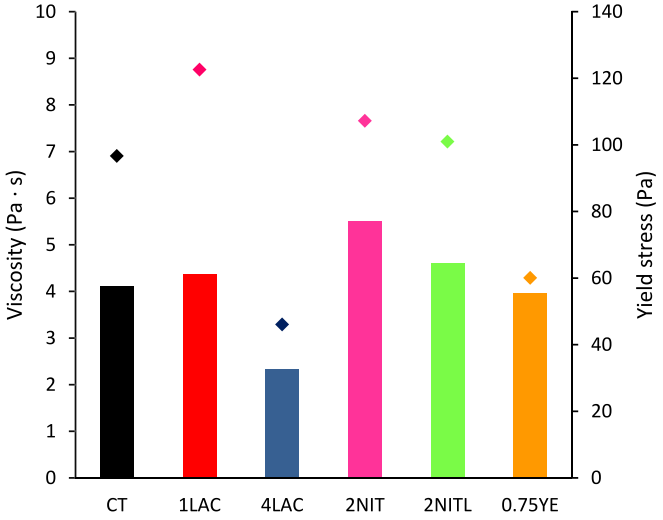

Fig. 9. Viscosity and yield stress measured at 3 min after water to cement contact.

These results agreed with the trends obtained in the previous section, as these pastes (4LAC and 0.75YE) reached the maximum torque minutes after hydration began rather than at the time the FCT was developed.

3.5. Analysis of Fourier transform infrared spectroscopy (FTIR)

The flow behaviour evolution of the 4LAC and 0.75YE pastes exhibited similarities, as shown in Fig. 8. Monitoring of their early hydration in the rheometer showed an increase in torque after approximately 10 min, which was not observed for the remaining pastes. The previous sections revealed that the rheological performance of the 4LAC paste is likely related to the enhancement of ettringite precipitation at the beginning of the reaction. However, insufficient information was provided on the rheological performance of the 0.75YE paste. Therefore, these pastes were investigated by performing infrared analysis after 15 min and 4 h of hydration, the results of which are shown in Fig. 10.

Both spectra were dominated by calcite peaks, primarily derived from the limestone filler and, to a lesser extent, from the starting cement. The peaks at 1405, 872, and 711 cm^{-1}, corresponding to the asymmetric C-O bond stretching and out-of-plane and in-plane bending vibrations of the O-C-O bonds, respectively, can be assigned to this compound [81,82]. Another common aspect of the two samples was the vibrations attributable to calcium silicates (alite and belite), associated with the peaks at 922 and 515 cm^{-1} (arising from the asymmetric Si-O bond stretching and ν_4 bending of the O-Si-O bonds, respectively). The weak peak at 465 cm^{-1} (ν_4 bending of the O-Si-O bonds) could also be attributed to these compounds [81,83].

There were two main differences between the spectra of the 4LAC and 0.75YE pastes. The first was the peak at 1578 cm^{-1} in the 4LAC paste spectrum arising from the asymmetric stretching vibration of the C═O bond of the lactate carboxyl group [84]. However, the greatest difference occurs in the regions related to the vibrations originating from the sulphate groups, which were particularly noticeable in the area associated with the S-O stretches, located in the 1000–1200 cm^{-1} range. The 0.75YE paste featured multiple peaks in this region, but only the ones at 1124 and 1137 cm^{-1} can be attributed to gypsum. In contrast, the peak at 1195 cm^{-1} and the shoulder at 1105 cm^{-1} indicate the presence of significant amounts of syngenite. The peaks at 1124 and 1137 cm^{-1}, coincident with those of gypsum, could also be attributed to syngenite [82]. In contrast, this zone of the 4LAC paste spectrum was dominated by the signal at 1120 cm^{-1}, which is distinctive of the S-O vibration of ettringite. However, syngenite peaks are also observed. The evolution of the spectra after 4 h of hydration (Fig. 10) revealed that the peaks attributed to syngenite became weaker as the reaction progressed for the 4LAC paste, whereas for the 0.75YE paste, they intensified considerably.

Syngenite formation in the pastes was expected due to the dissolution of readily soluble arcanite at the beginning of hydration, which increased the dissolved content of potassium and sulphate ions. This phenomenon is bound to be enhanced in pastes with lower reactivity, such as 0.75YE, where an excess of calcium ions is available in the solution, as they are not efficiently consumed to give rise to cement hydration products. Therefore, syngenite in these pastes acted as a secondary source of sulphate ions, which would explain the delay between gypsum consumption and the onset of the sulphate depletion peak reported in section 3.2.3 for 0.75YE.

The development of syngenite in cements containing potassium sulphate has been well-documented in the literature [74]. Moreover, several researchers have linked syngenite crystallisation during the early stages of hydration, in the form of long prismatic crystals, to the torque increase and paste stiffening, as reported in Section 3.4 [74,75,85,86].

4. Conclusions

In this study, the influence of three commonly used nutrients in the field of self-healing has been analysed. Throughout the combination of XRD techniques alongside with calorimetry measurements, it was possible to determine the chemical composition arising during the hydration processes when these nutrients are incorporated. Additionally, the research was complemented by a rheological study and by setting time techniques, which contributes to a comprehensive understanding of the overall effect of each nutrient at early ages.

The addition of **lactate** caused notable changes in the reaction of the aluminates, generating a greater amount of ettringite at the beginning of the reaction. This correlates with the rheological behaviour observed during the fluidity test. The silicate reaction shows a notable delay when 4% lactate was added. Once the reaction of the silicates had elapsed, the excess ettringite generated at the beginning of hydration was destabilised leading to the formation of a greater quantity of AFm phases prior to its formation in the control paste.

The addition of **nitrate** accelerated the hydration process, as verified by the Vicat results. Nevertheless, the XRD results did not show a greater or faster reaction of silicates. The main difference was the initial amount of gypsum, which was increased owing to the dissolution of arcanite present in the cement and the contribution of calcium ions introduced into the solution. Unlike the case of lactate, where the extra calcium promoted the formation of ettringite with nitrate, it favoured the formation of secondary gypsum. The incorporation of both salts simultaneously generated a behaviour much more similar to that of 1LAC than to the one of 2NIT, as determined by the XRD results and the heat-flow curves.

As expected, the incorporation of **yeast extract** notably inhibited the silicate reaction, even when it was added in small amounts, as the one studied here. Similar to silicates, the reaction of aluminates was negatively affected. This low reaction activity, in addition to the presence of

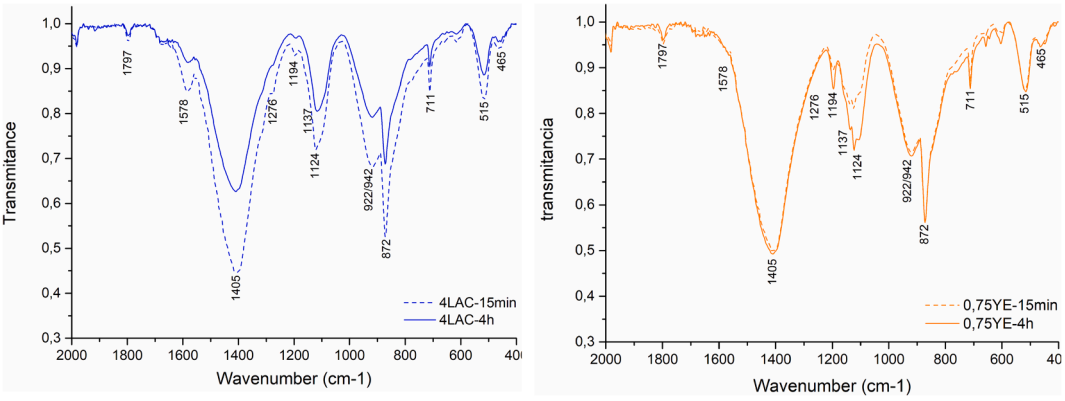

Fig. 10. FTIR spectrum of the 4LAC mixture (left) and 0.75YE mixture (right).

arcanite in anhydrous cement, favoured the possible formation of syngenite in the mixture and explained the observed rheological behaviour.

The addition of these nutrients had notable effects on the rheological properties and hydration processes, possibly limiting their use for certain applications. This, along with long-term alterations and the behaviour when nutrients and bacteria are added together, require further research. Furthermore, the employment of another type of nutrients or another mix compositions would also be interesting, especially to better understand the factor effect of lactate concentration.

CRediT authorship contribution statement

Adonay Pinto: Conceptualization, Formal analysis, Investigation, Visualization, Writing – original draft. **Belén González-Fonteboa:** Formal analysis, Investigation, Supervision, Writing – review & editing. **Sindy Seara-Paz:** Formal analysis, Investigation, Supervision, Writing – review & editing. **Fernando Martínez-Abella:** Investigation, Supervision, Writing – review & editing.

Declaration of Competing Interest

The authors declare that they have no known competing financial interests or personal relationships that could have appeared to influence the work reported in this paper.

Data availability

Data will be made available on request.

Acknowledgements

This work has been carried out within the framework of the following projects: “Design of sustainable concrete for 3D printing based on rheology and on the control of very early properties (Eco3DConcrete)- [PID2020-115433RB-I00]”, “Design of concrete precast elements incorporating sustainable strategies for self-healing to increase their service life (PREHEALING)- [PDC2021-121660-I00]” and “Exploiting the synergic effects between 3D printing and self-healing technologies to design sustainable and durable concrete (3DHealConcrete) [TED2021-129757B-I00]” all funded by MINECO (Ministry of Economy, Industry and Competitiveness).

In addition, the authors would like to thank the Xunta de Galicia (Spain) for the financial support through its pre-doctoral contracts program.

References

[1] C. Liu, Z. Lv, J. Xiao, X. Xu, X. Nong, H. Liu, On the mechanism of Cl− diffusion transport in self-healing concrete based on recycled coarse aggregates as microbial carriers, Cem. Concr. Compos. 124 (2021) 104232.
[2] R.A. Khushnood, Z.A. Qureshi, N. Shaheen, S. Ali, Bio-mineralized self-healing recycled aggregate concrete for sustainable infrastructure, Sci. Total Environ. 703 (2020), 135007, https://doi.org/10.1016/j.scitotenv.2019.135007.
[3] L. Jiang, G. Jia, Y. Wang, Z. Li, Optimization of Sporulation and Germination Conditions of Functional Bacteria for Concrete Crack-Healing and Evaluation of their Repair Capacity, ACS Appl. Mater. Interfaces 12 (2020) 10938–10948, https://doi.org/10.1021/acsami.9b21465.
[4] A. Al-Tabbaa, C. Litina, P. Giannaros, A. Kanellopoulos, L. Souza, First UK field application and performance of microcapsule-based self-healing concrete, Constr. Build. Mater. 208 (2019) 669–685, https://doi.org/10.1016/j.conbuildmat.2019.02.178.
[5] S. Mahmoodi, P. Sadeghian, Self-healing concrete: A review of recent research developments and existing research gaps, Proceedings, Annu. Conf. - Can. Soc. Civ. Eng. 2019-June (2019) 1–10.
[6] Z. Li, C. Leung, Y. Xi, Structural renovation in concrete, 2009. https://doi.org/10.1201/9781482265972.
[7] M. Seifan, A.K. Sarmah, A.K. Samani, A. Ebrahiminezhad, Y. Ghasemi, A. Berenjian, Mechanical properties of bio self-healing concrete containing immobilized bacteria with iron oxide nanoparticles, Appl. Microbiol. Biotechnol. 102 (2018) 4489–4498, https://doi.org/10.1007/s00253-018-8913-9.
[8] O. Hamza, M. Esaker, D. Elliott, A. Souid, The effect of soil incubation on bio self-healing of cementitious mortar, Mater. Today Commun. 24 (2020) 100988.
[9] B. Balzano, J. Sweeney, G. Thompson, C.L. Tuinea-Bobe, A. Jefferson, Enhanced concrete crack closure with hybrid shape memory polymer tendons, Eng. Struct. 226 (2021), 111330, https://doi.org/10.1016/j.engstruct.2020.111330.
[10] W. Pungrasmi, J. Intarasoontron, P. Jongvivatsakul, S. Likitlersuang, Evaluation of Microencapsulation Techniques for MICP Bacterial Spores Applied in Self-Healing Concrete, Sci. Rep. 9 (2019) 1–10, https://doi.org/10.1038/s41598-019-49002-6.
[11] W. Zhang, Q. Zheng, A. Ashour, B. Han, Self-healing cement concrete composites for resilient infrastructures: A review, Compos. B Eng. 189 (2020) 107892.
[12] S. Mondal, A. (Dey) Ghosh, Spore-forming Bacillus subtilis vis-à-vis non-spore-forming Deinococcus radiodurans, a novel bacterium for self-healing of concrete structures: A comparative study, Constr. Build. Mater. 266 (2021), 121122, https://doi.org/10.1016/j.conbuildmat.2020.121122.
[13] S. Joshi, S. Goyal, A. Mukherjee, M.S. Reddy, Protection of concrete structures under sulfate environments by using calcifying bacteria, Constr. Build. Mater. 209 (2019) 156–166, https://doi.org/10.1016/j.conbuildmat.2019.03.079.
[14] T.H. Nguyen, E. Ghorbel, H. Fares, A. Cousture, Bacterial self-healing of concrete and durability assessment, Cem. Concr. Compos. 104 (2019), 103340, https://doi.org/10.1016/j.cemconcomp.2019.103340.
[15] N. De Belie, E. Gruyaert, A. Al-Tabbaa, P. Antonaci, C. Baera, D. Bajare, A. Darquennes, R. Davies, L. Ferrara, T. Jefferson, C. Litina, B. Miljevic, A. Otlewska, J. Ranogajec, M. Roig-Flores, K. Paine, P. Lukowski, P. Serna, J. M. Tulliani, S. Vucetic, J. Wang, H.M. Jonkers, A Review of Self-Healing Concrete for Damage Management of Structures, Adv. Mater. Interfaces 5 (2018) 1–28, https://doi.org/10.1002/admi.201800074.
[16] R. Jakubovskis, A. Jankutė, J. Urbonavičius, V. Gribniak, Analysis of mechanical performance and durability of self-healing biological concrete, Constr. Build. Mater. 260 (2020) 119822.
[17] N. De Belie, J. Wang, Z.B. Bundur, K. Paine, Bacteria-based concrete, Elsevier Ltd, 2018. https://doi.org/10.1016/B978-0-08-102181-1.00019-8.
[18] M. Zamani, S. Nikafshar, A. Mousa, A. Behnia, Bacteria encapsulation using synthesized polyurea for self-healing of cement paste, Constr. Build. Mater. 249 (2020), 118556, https://doi.org/10.1016/j.conbuildmat.2020.118556.
[19] N. De Belie, J. Wang, Bacteria-based repair and self-healing of concrete, J. Sustain. Cem. Mater. 5 (2015) 35–56, https://doi.org/10.1080/21650373.2015.1077754.
[20] X. Chen, J. Yuan, M. Alazhari, Effect of Microbiological Growth Components for Bacteria-Based self healing on the properties of cement mortar, Materials (Basel) 12 (8) (2019) 1303.
[21] H.M. Jonkers, A. Thijssen, G. Muyzer, O. Copuroglu, E. Schlangen, Application of bacteria as self-healing agent for the development of sustainable concrete, Ecol. Eng. 36 (2010) 230–235, https://doi.org/10.1016/j.ecoleng.2008.12.036.
[22] K. Vijay, M. Murmu, S.V. Deo, Bacteria based self healing concrete – A review, Constr. Build. Mater. 152 (2017) 1008–1014, https://doi.org/10.1016/j.conbuildmat.2017.07.040.
[23] M. Luo, C. Qian, Influences of bacteria-based self-healing agents on cementitious materials hydration kinetics and compressive strength, Constr. Build. Mater. 121 (2016) 659–663, https://doi.org/10.1016/j.conbuildmat.2016.06.075.
[24] P. Ryparová, P. Tesárek, H. Schreiberová, Z. Prošek, The effect of temperature on bacterial self-healing processes in building materials, IOP Conf. Ser. Mater. Sci. Eng. 726 (1) (2020) 012012.
[25] L. Skevi, B.J. Reeksting, T.D. Hoffmann, S. Gebhard, K. Paine, Incorporation of bacteria in concrete: The case against MICP as a means for strength improvement, Cem. Concr. Compos. 120 (2021), 104056, https://doi.org/10.1016/j.cemconcomp.2021.104056.
[26] P. Ryparová, Z. Prošek, H. Schreiberová, P. Bílý, P. Tesárek, The role of bacterially induced calcite precipitation in self-healing of cement paste, J. Build. Eng. 39 (2021) 102299.
[27] S. Gupta, Comparison of improved autogenous and bio-based self-healing techniques in fiber-reinforced mortar: Effect of bacteria incorporation strategy and fiber hybridization, J. Build. Eng. 45 (2022), 103607, https://doi.org/10.1016/j.jobe.2021.103607.
[28] R. Roy, E. Rossi, J. Silfwerbrand, H. Jonkers, Self-healing capacity of mortars with added-in bio-plastic bacteria-based agents: Characterization and quantification through micro-scale techniques, Constr. Build. Mater. 297 (2021), 123793, https://doi.org/10.1016/j.conbuildmat.2021.123793.
[29] K.M. Osman, F.M. Taher, A. Abd EL-Tawab, A.S. Faried, Role of different microorganisms on the mechanical characteristics, self-healing efficiency, and corrosion protection of concrete under different curing conditions, J. Build. Eng. 41 (2021) 102414.
[30] J. García-González, P. Faria, A.S. Pereira, P.C. Lemos, J.M. Morán-del Pozo, M. I. Guerra-Romero, A. Juan-Valdés, Sustainable cement mortar bioformulated with a bioproduct obtained from fermentation of biodiesel’ crude glycerol, J. Clean. Prod. 313 (2021) 127885.
[31] Z. Basaran Bundur, M.J. Kirisits, R.D. Ferron, Biomineralized cement-based materials: Impact of inoculating vegetative bacterial cells on hydration and strength, Cem. Concr. Res. 67 (2015) 237–245, https://doi.org/10.1016/j.cemconres.2014.10.002.
[32] H. Schreiberová, P. Bílý, J. Fládr, K. Šeps, R. Chylík, T. Trtík, Impact of the self-healing agent composition on material characteristics of bio-based self-healing concrete, Case Stud. Constr. Mater. 11 (2019) e00250.
[33] A.R. Suleiman, A.J. Nelson, M.L. Nehdi, Visualization and quantification of crack self-healing in cement-based materials incorporating different minerals, Cem. Concr. Compos. 103 (2019) 49–58, https://doi.org/10.1016/j.cemconcomp.2019.04.026.
[34] L. Tan, B. Reeksting, V. Ferrandiz-Mas, A. Heath, S. Gebhard, K. Paine, Effect of carbonation on bacteria-based self-healing of cementitious composites, Constr.

Build. Mater. 257 (2020), 119501, https://doi.org/10.1016/j.conbuildmat.2020.119501.
[35] B.J. Reeksting, T.D. Hoffmann, L. Tan, K. Paine, S. Gebhard, EMIn-depth profiling of calcite precipitation by environmental bacteria reveals fundamental mechanistic differences with relevance to application, BioRxiv. 86 (2019) 1–16, https://doi.org/10.1101/850883.
[36] J. Xu, Y. Tang, X. Wang, A correlation study on optimum conditions of microbial precipitation and prerequisites for self-healing concrete, Process Biochem. 94 (2020) 266–272, https://doi.org/10.1016/j.procbio.2020.04.028.
[37] P. Risdanareni, L. Ma, J. Wang, N. De Belie, Suitable yeast extract concentration for the production of self-healing mortar with expanded clay as bacterial carrier, Mater. Constr. 72 (348) (2022) e296.
[38] M. Vaezi, S.A. Zareei, M. Jahadi, Recycled microbial mortar: Effects of bacterial concentration and calcium lactate content, Constr. Build. Mater. 234 (2020), 117349, https://doi.org/10.1016/j.conbuildmat.2019.117349.
[39] I. Jang, D. Son, W. Kim, W. Park, C. Yi, Effects of spray-dried co-cultured bacteria on cement mortar, Constr. Build. Mater. 243 (2020), 118206, https://doi.org/10.1016/j.conbuildmat.2020.118206.
[40] Á. González, A. Parraguez, L. Corvalán, N. Correa, J. Castro, C. Stuckrath, M. González, Evaluation of Portland and Pozzolanic cement on the self-healing of mortars with calcium lactate and bacteria, Constr. Build. Mater. 257 (2020) 1–11, https://doi.org/10.1016/j.conbuildmat.2020.119558.
[41] S.K. Chaerun, R. Syarif, R.K. Wattimena, Bacteria incorporated with calcium lactate pentahydrate to improve the mortar properties and self-healing occurrence, Sci. Rep. 10 (2020) 1–9, https://doi.org/10.1038/s41598-020-74127-4.
[42] Y. Su, C. Qian, Y. Rui, J. Feng, Exploring the coupled mechanism of fibers and bacteria on self-healing concrete from bacterial extracellular polymeric substances (EPS), Cem. Concr. Compos. 116 (2021), 103896, https://doi.org/10.1016/j.cemconcomp.2020.103896.
[43] K. Scrivener, R. Snellings, B. Lothenbach, A Practical Guide to Microstructural Analysis of Cementitious Materials, 2018. https://doi.org/10.1201/b19074.
[44] S.T. Bergold, F. Goetz-Neunhoeffer, J. Neubauer, Quantitative analysis of C-S-H in hydrating alite pastes by in-situ XRD, Cem. Concr. Res. 53 (2013) 119–126, https://doi.org/10.1016/j.cemconres.2013.06.001.
[45] C. Hesse, F. Goetz-Neunhoeffer, J. Neubauer, A new approach in quantitative in-situ XRD of cement pastes: Correlation of heat flow curves with early hydration reactions, Cem. Concr. Res. 41 (2011) 123–128, https://doi.org/10.1016/j.cemconres.2010.09.014.
[46] S. Dittrich, J. Neubauer, F. Goetz-Neunhoeffer, The influence of fly ash on the hydration of OPC within the first 44 h - A quantitative in situ XRD and heat flow calorimetry study, Cem. Concr. Res. 56 (2014) 129–138, https://doi.org/10.1016/j.cemconres.2013.11.013.
[47] N. Doebelin, R. Kleeberg, Profex: A graphical user interface for the Rietveld refinement program BGMN, J. Appl. Cryst. 48 (2015) 1573–1580, https://doi.org/10.1107/S1600576715014685.
[48] D. Jansen, F. Goetz-Neunhoeffer, C. Stabler, J. Neubauer, A remastered external standard method applied to the quantification of early OPC hydration, Cem. Concr. Res. 41 (2011) 602–608, https://doi.org/10.1016/j.cemconres.2011.03.004.
[49] K. Hurle, J. Neubauer, M. Bohner, N. Doebelin, F. Goetz-Neunhoeffer, Calorimetry investigations of milled α-tricalcium phosphate (α-TCP) powders to determine the formation enthalpies of α-TCP and X-ray amorphous tricalcium phosphate, Acta Biomater. 23 (2015) 338–346, https://doi.org/10.1016/j.actbio.2015.05.026.
[50] D. Jansen, C. Stabler, F. Goetz-Neunhoeffer, S. Dittrich, J. Neubauer, Does Ordinary Portland Cement contain amorphous phase? A quantitative study using an external standard method, Powder Diffr. 26 (2011) 31–38, https://doi.org/10.1154/1.3549186.
[51] D. Jansen, F. Goetz-Neunhoeffer, B. Lothenbach, J. Neubauer, The early hydration of Ordinary Portland Cement (OPC): An approach comparing measured heat flow with calculated heat flow from QXRD, Cem. Concr. Res. 42 (2012) 134–138, https://doi.org/10.1016/j.cemconres.2011.09.001.
[52] Z. Duan, S. Hou, J. Xiao, A. Singh, Rheological properties of mortar containing recycled powders from construction and demolition wastes, Constr. Build. Mater. 237 (2020), 117622, https://doi.org/10.1016/j.conbuildmat.2019.117622.
[53] K. Fang, D. Zhang, D. Wang, Z. Liu, M. Zhang, S. Zhang, The impact of coal gasification slag powder on fluidity, rheology and viscoelasticity properties of fresh cement paste, J. Build. Eng. 69 (2023), 106237, https://doi.org/10.1016/j.jobe.2023.106237.
[54] Q. Zhong, H. Nie, G. Xie, H. Peng, Experimental study on the characteristics, rheological factors, and flowability of MK-GGBFS geopolymer slurry, J. Build. Eng. 76 (2023), 107300, https://doi.org/10.1016/j.jobe.2023.107300.
[55] D. Snoeck, L.F. Velasco, A. Mignon, S. Van Vlierberghe, P. Dubruel, P. Lodewyckx, N. De Belie, The influence of different drying techniques on the water sorption properties of cement-based materials, Cem. Concr. Res. 64 (2014) 54–62, https://doi.org/10.1016/j.cemconres.2014.06.009.
[56] J. Bensted, P. Barnes, Structure and performance of cements, 2002.
[57] O. Chaudhari, J.J. Biernacki, S. Northrup, Effect of carboxylic and hydroxycarboxylic acids on cement hydration: experimental and molecular modeling study, J. Mater. Sci. 52 (2017) 13719–13735, https://doi.org/10.1007/s10853-017-1464-0.
[58] J. Cheung, A. Jeknavorian, L. Roberts, D. Silva, Impact of admixtures on the hydration kinetics of Portland cement, Cem. Concr. Res. 41 (2011) 1289–1309, https://doi.org/10.1016/j.cemconres.2011.03.005.
[59] M. Palou, M. Boháč, E. Kuzielová, R. Novotný, M. Žemlička, J. Dragomirová, Use of calorimetry and thermal analysis to assess the heat of supplementary cementitious materials during the hydration of composite cementitious binders, J. Therm. Anal. Calorim. 142 (2020) 97–117, https://doi.org/10.1007/s10973-020-09341-3.
[60] T. Dorn, T. Hirsch, D. Stephan, Analyzing the early structural build-up of accelerated cement pastes, Mater. Struct. Constr. 54 (2021), https://doi.org/10.1617/s11527-021-01662-5.
[61] S. Bergold, S. Metallic, P. Gmbh, D. Jansen, S. Dittrich, Development of C-S-H during the early hydration of alite with water at different temperatures : direct quantification by in-situ XRD, GDCh-Monographie (2012), 45 (Tagung Bauchemie, 2012), 91-96.
[62] J.W. Bullard, H.M. Jennings, R.A. Livingston, A. Nonat, G.W. Scherer, J. S. Schweitzer, K.L. Scrivener, J.J. Thomas, Mechanisms of cement hydration, Cem. Concr. Res. 41 (2011) 1208–1223, https://doi.org/10.1016/j.cemconres.2010.09.011.
[63] G.V. Bakore, S.D. Bhardwaj, Spectrophotometric Study of Iron(III)-Lactate Complex and its Photo-reduction, Zeitschrift Für Phys, Chemie. 227O (1964) 26–32, https://doi.org/10.1515/zpch-1964-22706.
[64] R. Portanova, L.H.J. Lajunen, M. Tolazzi, J. Piispanen, Critical evaluation of stability constants for α-hydroxycarboxylic acid complexes with protons and metal ions and the accompanying enthalpy changes: Part II. Aliphatic 2-hydroxycarboxylic acids (IUPAC technical report), Pure Appl. Chem. 75 (2003) 495–540, https://doi.org/10.1351/pac200375040495.
[65] P. Cardiano, R.M. Cigala, F. Crea, F. Giacobello, O. Giuffrè, A. Irto, G. Lando, S. Sammartano, Sequestration of Aluminium(III) by different natural and synthetic organic and inorganic ligands in aqueous solution, Chemosphere 186 (2017) 535–545, https://doi.org/10.1016/j.chemosphere.2017.08.015.
[66] H. Justnes, E.C. Nygaard, Technical calcium nitrate as set accelerator for cement at low temperatures, Cem. Concr. Res. 25 (1995) 1766–1774, https://doi.org/10.1016/0008-8846(95)00172-7.
[67] W. Kunther, B. Lothenbach, J. Skibsted, Influence of the Ca/Si ratio of the C-S-H phase on the interaction with sulfate ions and its impact on the ettringite crystallization pressure, Cem. Concr. Res. 69 (2015) 37–49, https://doi.org/10.1016/j.cemconres.2014.12.002.
[68] M. Balonis, M. Mędala, F.P. Glasser, Influence of calcium nitrate and nitrite on the constitution of AFm and AFt cement hydrates, Adv. Cem. Res. 23 (2011) 129–143, https://doi.org/10.1680/adcr.10.00002.
[69] B. Lothenbach, D.A. Kulik, T. Matschei, M. Balonis, L. Baquerizo, B. Dilnesa, G. D. Miron, R.J. Myers, Cemdata18: A chemical thermodynamic database for hydrated Portland cements and alkali-activated materials, Cem. Concr. Res. 115 (2019) 472–506, https://doi.org/10.1016/j.cemconres.2018.04.018.
[70] D. Marchon, S. Kawashima, H. Bessaies-Bey, S. Mantellato, S. Ng, Hydration and rheology control of concrete for digital fabrication: Potential admixtures and cement chemistry, Cem. Concr. Res. 112 (2018) 96–110, https://doi.org/10.1016/j.cemconres.2018.05.014.
[71] M. Collepardi, S. Monosi, G. Moriconi, M. Pauri, Influence of gluconate, lignosulfonate or glucose on the C3A hydration in the presence of gypsum with or without lime, Cem. Concr. Res. 14 (1984) 105–112, https://doi.org/10.1016/0008-8846(84)90086-3.
[72] M. Collepardi, S. Monosi, G. Moriconi, M. Pauri, Influence of Gluconate, Lignosulfonate, and Glucose Admixtures on the Hydration of Tetracalcium Aluminoferrite in the Presence of Gypsum with or without Calcium Hydroxide, J. Am. Ceram. Soc. 68 (5) (1985) C-126–C-128.
[73] N. Chikh, M. Cheikh-Zouaoui, S. Aggoun, R. Duval, Effects of calcium nitrate and triisopropanolamine on the setting and strength evolution of Portland cement pastes, Mater. Struct. Constr. 41 (2008) 31–36, https://doi.org/10.1617/s11527-006-9215-8.
[74] C.-W. Chung, J.-Y. Lee, Premature Stiffening of Cement Paste Caused by Secondary Gypsum and Syngenite Formation (False Set), Archit. Res. 13 (2011) 25–32, https://doi.org/10.5659/aikar.2011.13.1.25.
[75] C. Rößler, A. Eberhardt, H. Kučerová, B. Möser, Influence of hydration on the fluidity of normal Portland cement pastes, Cem. Concr. Res. 38 (2008) 897–906, https://doi.org/10.1016/j.cemconres.2008.03.003.
[76] C.W. Chung, P. Suraneni, J.S. Popovics, L.J. Struble, Using ultrasonic wave reflection to monitor false set of cement paste, Cem. Concr. Compos. 84 (2017) 10–18, https://doi.org/10.1016/j.cemconcomp.2017.08.010.
[77] C. Jakob, D. Jansen, N. Ukrainczyk, E. Koenders, U. Pott, D. Stephan, J. Neubauer, Relating ettringite formation and rheological changes during the initial cement hydration: A comparative study applying XRD analysis, rheological measurements and modeling, Materials (Basel). 12 (18) (2019) 2957.
[78] J.d.S. Andrade Neto, A.G. De la Torre, A.P. Kirchheim, Effects of sulfates on the hydration of Portland cement – A review, Constr. Build. Mater. 279 (2021) 122428.
[79] J.S. Andrade Neto, P.R. de Matos, A.G. De la Torre, C.E.M. Campos, P.J.P. Gleize, P. J.M. Monteiro, A.P. Kirchheim, The role of sodium and sulfate sources on the rheology and hydration of C3A polymorphs, Cem. Concr. Res. 151 (2022) 106639.
[80] F. Martirena, Y. Rodriguez-Rodriguez, A. Callico, R. Gonzalez, Y. Diaz, G. Bracho, A. Alujas, J.O. Guerra De Leon, Y. Alvarado-Capó, Microorganism-based bioplasticizer for cementitious materials, Constr. Build. Mater. 60 (2014) 91–97, https://doi.org/10.1016/j.conbuildmat.2014.02.063.
[81] K. Nakamoto, Infrared and raman spectra of inorganic and coordination compounds, 4th ed., John Wiley and Sons, 1986.
[82] N. V. Chukanov, A.D. Chervonnyi, IR Spectra of Minerals and Reference Samples Data, in: Infrared Spectrosc. Miner. Relat. Compd., Springer, 2014: pp. 21–1701. https://doi.org/https://doi.org/10.1007/978-3-319-25349-7.
[83] L. Fernández-Carrasco, D. Torrens-Martín, L.M. Morales, S. Martínez-Ramírez, Infrared Spectroscopy in the Analysis of Building and Construction Materials, in: T. Theophile (Ed.), Infrared Spectrosc. - Mater. Sci. Eng. Technol., InTech, 2012: pp. 369–382. https://doi.org/10.5772/36186.

[84] I.S. Yoon, G.-W. Lee, H.J. Lee, S.H. Park, S.Y. Park, S.G. Lee, J.-S. Kim, M.S. Heu, Characterization of Calcium Lactate Prepared from Butter Clam Saxidomus purpuratus Shell Powder, Korean, J. Fish. Aquat. Sci. 49 (3) (2016) 301–309.
[85] L. Huang, P. Yan, Y. Liu, Effect of alkali content in cement on the fluidity and structural build-up of plasticized cement pastes, Constr. Build. Mater. 253 (2020), 119180, https://doi.org/10.1016/j.conbuildmat.2020.119180.
[86] S. Smillie, E. Moulin, D.E. Macphee, F.P. Glasser, J. Bensted, Freshness of cement: Conditions for syngenite CaK2(SO4)2 · H2O formation, Adv. Cem. Res. 6 (1994) 135–137, https://doi.org/10.1680/adcr.1994.6.23.135.